

## Three Dimensional Simulations of Diesel Sprays Using n-Dodecane as a Surrogate

*S. Som<sup>1</sup>, D.E. Longman<sup>1</sup>, Z. Luo<sup>2</sup>, M. Plomer<sup>2</sup>, T. Lu<sup>2</sup>*

<sup>1</sup>*Transportation Technology Research and Development Center, Argonne National Laboratory,  
Argonne, Illinois 60439, USA*

<sup>2</sup>*Department of Mechanical Engineering, University of Connecticut,  
Storrs, Connecticut 06269-3139, USA*

Three dimensional simulations of ignition and combustion diesel lifted flames were conducted in a constant volume combustion chamber under engine-like conditions with turbulence. These simulations were performed to mimic the recent experiments at Sandia National Laboratory with n-dodecane as a surrogate for diesel fuel. In the first step, the spray models were validated using the data for liquid length and spray penetration. A skeletal mechanism was then developed for the 3-D simulations with a skeletal mechanism with 103 species and 370 reactions derived from a detailed mechanism consisting of 2115 species and 8157 reactions developed by the Lawrence Livermore National Laboratory. The mechanism reduction was performed with an algorithm combining direct relation graph with expert knowledge (DRG-X) and sensitivity analysis. The skeletal mechanism was derived from and extensively validated for conditions relevant to engine combustion, using auto-ignition, jet stirred reactor (JSR), and counter flow diffusion flames. The mechanism was able to satisfactorily predict various combustion characteristics such as ignition delay, flame lift-off length, and equivalence ratios of 0.5-2.0.

### 1. Introduction

Diesel fuel has been extensively used world-wide for heavy-duty transportation applications. Traditionally, diesel fuel has been represented by n-heptane (NHPT) as a surrogate [1,2,3]. However, since the average carbon content in diesel fuel ranges from 12 to 13, n-dodecane is being evaluated as a surrogate component for diesel fuel that may be more suitable than NHPT. Recently, detailed chemical kinetic models for n-alkanes up to dodecane has been developed by You et al. [4] for high temperature applications. The model has been validated against experiments of plug flow, jet stirred reactors (JSR), laminar flame speeds, and ignition delay times. Westbrook et al. [5] developed a detailed chemical kinetic mechanism for combustion of n-alkanes from n-octane to n-hexadecane consisting of 2115 species and 8157 reactions. This mechanism includes low temperature chemistry and was validated over a wide range of conditions [6].

The Engine Combustion Network (ECN) [7,8,9], which is dedicated to the improvement of computational fluid dynamics (CFD) modeling for compression ignition (CI) engines, recently conducted a series of measurements on the spray and combustion characteristics of n-dodecane. Since n-dodecane features similar boiling characteristics with diesel fuels, it is expected to better mimic the fuel-air mixing processes. This is of paramount importance since CI engine combustion is mixing controlled and NHPT (which is highly volatile) does not capture the mixing processes effectively. N-dodecane targets were called "Spray A" and the conditions are

noted in Table 1. Spray A experiments were conducted at a low-temperature combustion condition relevant to CI engines consisting of modern injection systems. Additionally, boundary conditions necessary for CFD simulations were carefully determined and the uncertainties were noted. This high-fidelity data-set [10] is now available for the modeling community to further develop the spray and combustion models for internal combustion engine applications. Extensive spray modeling has been performed using commercial softwares and open-source codes facilitating improvements in spray and turbulence modeling [11,12]. However, in the absence of a reliable chemical kinetic model for n-dodecane, thorough combustion modeling was not feasible.

CI engine processes are multi-physic, multi-scale and highly coupled in nature and involve turbulence, two-phase flows and complicated spray physics. Furthermore, turbulence-chemistry interactions, moving boundaries (piston and valves), heat-transfer (conduction, convection, and radiation), and complex combustion chemistry of fuel oxidation and emission formation make engine simulations a computationally daunting task. Accounting for detailed combustion chemistry in the order of hundreds of species and thousands of reactions is perhaps beyond the current computational capabilities. A major objective of the current study is to develop a reduced mechanism for n-dodecane from the detailed mechanism by Westbrook et al. [5]. An integrated reduction method combining directed relation graph (DRG) [13,14] with expert knowledge (DRG-X) [15] and DRG-aided sensitivity analysis (DRGASA) [16,17] was employed for mechanism reduction. Since a mechanism consisting of about 100 species and 500 reactions was recently integrated to a 3-D engine simulation [18]. We aim to obtain a comparable size reduced mechanism while retaining high chemical fidelity. Following gas-phase validations, the n-dodecane reduced mechanism will be implemented in a 3D engine modeling software called CONVERGE [19] for turbulent spray-combustion simulations.

The paper is organized in the following way. First the methodologies for mechanism reduction will be described. These reduction techniques will then be applied to the n-dodecane detailed mechanism to obtain a reduced mechanism which is applicable in the CI engine operating range. 3D turbulence spray-combustion modeling set-up will be described followed by a brief discussion about the underlying spray, combustion, and turbulence models, and the grid-generation strategy. The reduced mechanism will be validated with the detailed mechanism for homogeneous system including auto-ignition and perfectly stirred reactors (PSR). The reduced mechanism will also be validated against shock-tube, JSR, and counterflow flame data from the literature. Following the extensive validation, two-phase flow simulations at CI engine conditions will then be performed. Some details about the 3D constant volume spray combustion experiments performed at Sandia National Laboratory for the ECN workshop will also be described [8,9,10]. Lastly, robust validation against the spray and combustion data such as liquid length, vapor penetration, ignition delay, flame lift-off length (LOL), soot contours etc., will be performed.

## **2. Methodologies**

### **2.1 Mechanism Reduction**

The detailed mechanism for C8-C16 alkanes used in the present reduction was developed by the Lawrence Livermore National Laboratory (LLNL). It consists of 2115 and 8157 elementary reactions. To reduce this large mechanism for efficient numerical simulations, a recently

improved method of DRG, i.e. DRG with expert knowledge (DRG-X), is employed in the present work to eliminate unimportant species and reactions. DRG-X still features an overall linear reduction time and is fully automated. It further resolves the limitations of the original DRG and allows non-uniform reduction error for every species and heat release. By introducing expert knowledge in the DRG reduction, DRG-X can develop skeletal mechanisms of similar sizes but with higher chemical fidelity compared to those by DRG. Procedurally, species-specific x-values (the expert knowledge) are specified for selected species in addition to the starting species. The species associated with reactions with small uncertainties can be assigned a small x-value, say 0.1, and those with larger uncertainties can be assigned a larger x-value, say 0.3, while all the other species are assigned a default error tolerance, say 0.5. As a result, the errors in the skeletal mechanisms roughly match the level of uncertainties in the detailed mechanisms, such that the overall chemical fidelity can be retained in the skeletal mechanism. Moreover, for applications where some species of interest, e.g. a pollutant, need to be predicted with higher accuracy than that of the other species, small x-values can be specified for those species of interest. It is further noted that in DRG-X the x-value for heat release was included. The heat release was treated as a special species Q, with  $Q_i$  being the reaction heat for the  $i^{\text{th}}$  reaction. The effect of species elimination on heat release is further quantified as:

$$r_{QB} \equiv \frac{\max_i |Q_i \omega_i \delta_{Bi}|}{\max_i |Q_i \omega_i|}, \quad Q_i = -\sum_j \nu_{j,i} e_j \quad (1)$$

where  $e_j$  is the mole specific energy of the  $j^{\text{th}}$  species.  $\nu_{j,i}$  is the stoichiometric coefficient for the  $j^{\text{th}}$  species in the  $i^{\text{th}}$  reactions.  $\omega_i$  is the net reaction rates of the  $i^{\text{th}}$  reaction. Each term in the denominator is the contribution of a reaction to the heat release of the system, and the numerator consists of the terms in the denominator that involves species  $B$ . It is seen that the elimination of species  $B$  can significantly affect heat release if  $r_{QB}$  is larger than a user specified threshold value for temperature,  $\varepsilon_T$ . Since it is important to accurately predict heat release in many practical simulations, a small  $\varepsilon_T$  together with large  $\varepsilon_{\text{sp}}$  will be used in DRG-X.

In the present study, the reduction was performed based on reaction states sampled from auto-ignition and PSR for pressure of 1-100 atm, equivalence ratio of 0.5-2.0, and initial temperature of 700-1800 K for auto-ignition. The inlet temperature for PSR is 300K. Note that the NTC region which is important for auto-ignition under CI engine conditions was covered in the reduction. The starting species for the DRG-X is the  $H$  radical and temperature. By specifying  $\varepsilon_{\text{sp}} = 0.5$  and  $\varepsilon_T = 0.01$ , a skeletal mechanism with 369 species and 1495 reactions was obtained.

The method of DRGASA was subsequently applied to the 369-species mechanism. A worst-case relative error of 30% was specified for ignition delays and extinction time in PSR, almost every species was included in the global sensitivity analysis to ensure that the resulting mechanism is minimal in size. A skeletal mechanism with 103 species and 370 elementary reactions was eventually obtained.

## 2.2 Simulations of 3D Turbulent Spray Combustion

The 103-species skeletal mechanism was implemented in 3-D turbulent spray-combustion simulations for validation, in addition to the 0-D and 1-D simulations. The 3-D simulations were performed using the Eulerian-Lagrangian approach in the CFD software CONVERGE. It incorporates state-of-the-art models for spray injection, atomization and breakup, turbulence,

droplet collision, and coalescence. The gas-phase flow field is described using the Favre-Averaged Navier-Stokes equations in conjunction with the RNG k- $\epsilon$  turbulence model, which includes source terms for the effects of dispersed phase on gas-phase turbulence. These equations are solved using a finite volume solver. The details of these models can be found in previous publications [20,21,22,23], hence only a brief description is provided here.

Fuel injection is simulated using the blob injection model. Following the injection, Kelvin Helmholtz (KH) and Rayleigh Taylor (RT) models are used to predict the primary and secondary breakup of the computational parcels [24,25]. A breakup length is used within which the KH model is used to predict the primary breakup. Beyond the breakup length, the KH and RT models compete in breaking up the droplets. Droplet collisions are based on the no time counter algorithm [26]. Once collision occurs, the outcomes of the collision are predicted as bouncing, stretching, reflexively separating, or coalescing [27]. A droplet evaporation model based on the Frossling correlation is used in the present simulations. A dynamic drag model is also used postulating that the drag coefficient depends upon the shape of the droplet, which can vary between a sphere and a disk. The effects of turbulence on the droplet are also included, using a stochastic turbulent dispersion model. Kinetic modeling in CONVERGE is performed using the SAGE chemical kinetic solver [28], and is directly coupled with the gas-phase calculations using a well-stirred reactor model. The soot mass production within a computation cell is determined from a single-step competition between formation and oxidation rates of  $C_2H_2$  species based on the Hiroyasu model [29], which has been extensively used in engine-modeling literature.

CONVERGE uses an innovative, modified cut-cell Cartesian method for grid generation. The grid is generated internally to the code at runtime. For all cases, the base grid size was fixed at 2 mm. In order to resolve the flow near the injector, a fixed grid embedding is employed such that the minimum grid size is 0.25 mm. Apart from this region, it is rather difficult to determine *a priori* where a refined grid is needed. Hence, four levels of adaptive mesh refinement are employed for the velocity field. In order to match the combustion chamber geometry used in the experimental study [8,9], a cubical geometry of 108 mm on each side is generated (cf. Figure 1). The zoomed-in view of the fixed embedding region is also shown.

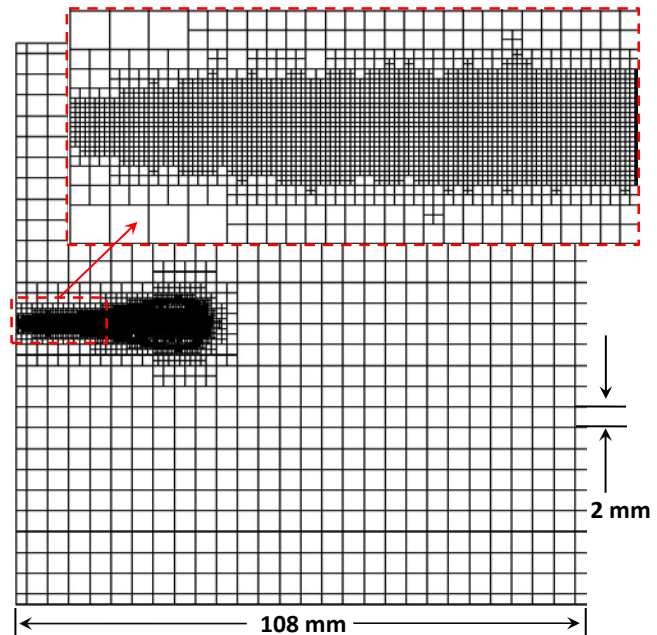


**Figure 1: Grid generated at 0.4 ms ASI for combusting sprays described in Table 1.**

### 3. Results and Discussion

The 103-species skeletal mechanism for n-dodecane was first validated against the detailed mechanism in homogeneous applications including auto-ignition and PSR. Figure 2a shows the ignition delay time as a function of initial temperature calculated using the detailed and skeletal

mechanisms for different pressures, equivalence ratios and initial temperatures covered in the reduction process. It can be observed in Fig. 2a that the skeletal mechanism matches quite well against the detailed mechanism under most of the conditions. Figure 2b further compares the temperature profiles of PSR calculated using the skeletal mechanism to that using the detailed mechanism, at various equivalence ratios and pressures. Good agreements were generally observed.

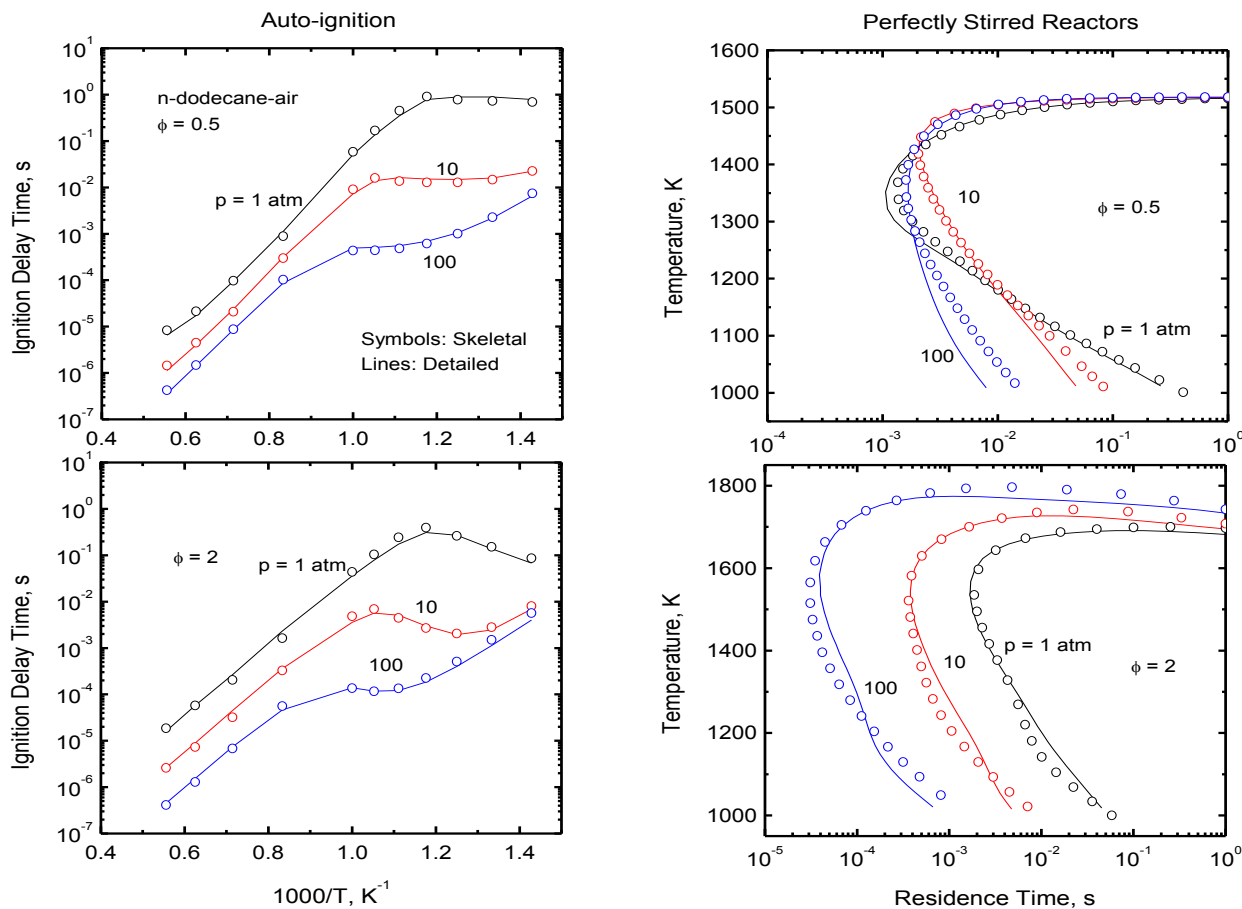


**Figure 2: Comparison of the 103-species skeletal mechanism with the detailed mechanism for n-dodecane-air, a) ignition delays, and b) extinction temperature profiles in PSR.**

### 3.1 Mechanism Validation against 0-D and 1-D Combustion Systems

The 103-species skeletal mechanism was then validated against the experimental measurements for homogeneous system including auto-ignition and JSR. Figure 3a compares the calculated ignition delay time for n-dodecane- $O_2$ -Ar mixture with the experiments [30,31] at various initial temperatures and pressures. It can be observed in Fig. 3a that the skeletal mechanism predicts the experimental trends of ignition delay fairly well. Figure 3b further shows the comparison between the calculated and measured ignition delay times for the n-dodecane-air mixture. The experimental data was obtained from Ref. [6]. The simulations agree well in trend with the experiments, including the NTC region.

The 103-species skeletal mechanism was further compared with the experimental measurements [32] of the thermal decomposition of n-dodecane in JSR. Figure 4a shows the

measured and calculated n-dodecane conversion percentage as a function of temperature in JSR. It is observed in Fig. 4a that the simulation predicted the measured data-sets fairly well. Figure 4b further compares the species profiles. It is seen that the skeletal mechanism shows good agreement with measurements, e.g. for the  $C_2H_4$  profile.

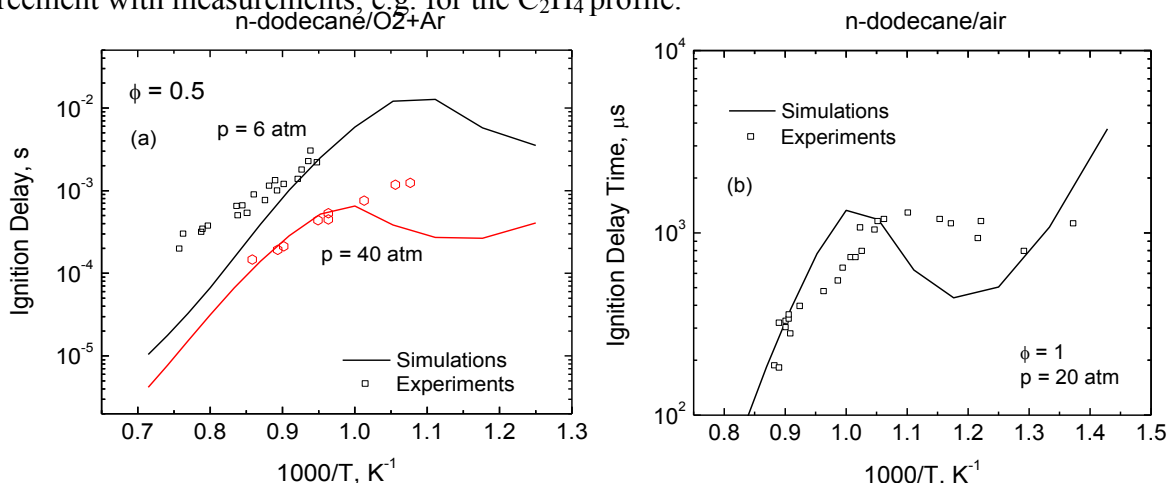


**Figure 3: Comparison of calculated and measured ignition delays of (a) n-dodecane/21%O<sub>2</sub>/Ar, at p = 6 and 40 atm and  $\phi = 0.5$ . Solid lines: simulation results, black symbols: experimental data from Ref. [31], red symbols: experimental data from Ref. [31]. (b) n-dodecane/air, at p = 20 atm and  $\phi = 1$ . Solid lines: simulation results, symbols: experimental data from Ref. [6].**

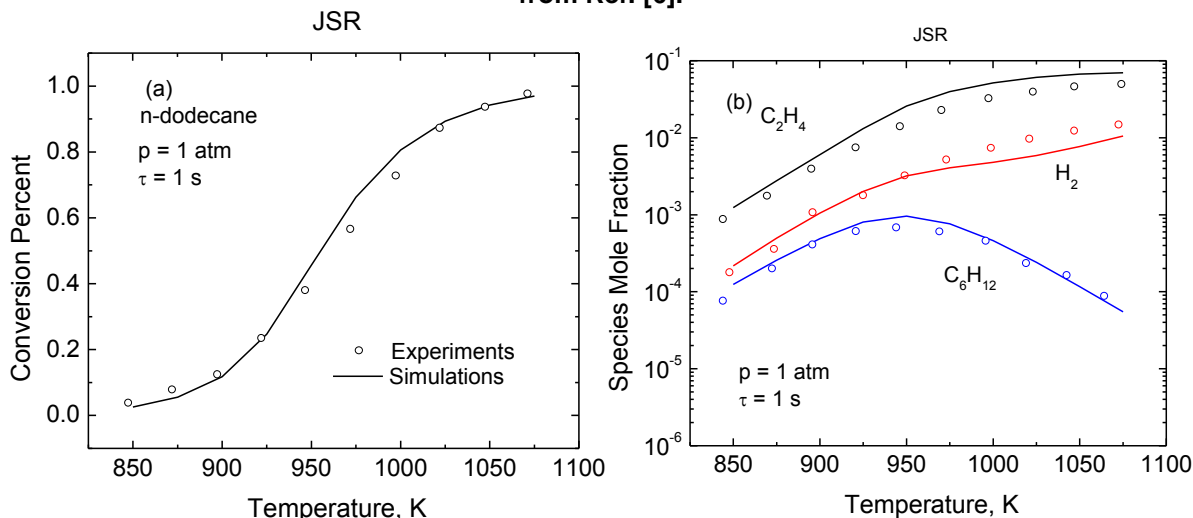


**Figure 4: Comparison of calculated and measured (a) conversion percent of n-dodecane thermal decomposition (b) species profiles, in JSR, at p = 1 atm and  $\tau = 1$  s. Solid lines: simulation results symbols: experimental data from [31].**

Next, the skeletal mechanism is validated for 1-D non-premixed flames. The results from the skeletal mechanism are shown in Figure 5, which plots the calculated temperature profiles with the skeletal mechanism along with the measured data by Cooke et al. [33] for a non-premixed counterflow flame of diluted n-dodecane mixture (1.5% n-dodecane and 98.5%N<sub>2</sub> in mole) at atmospheric pressure. The same boundary conditions from the experimental configuration were used for inlet temperatures, mixture compositions and flow velocities.

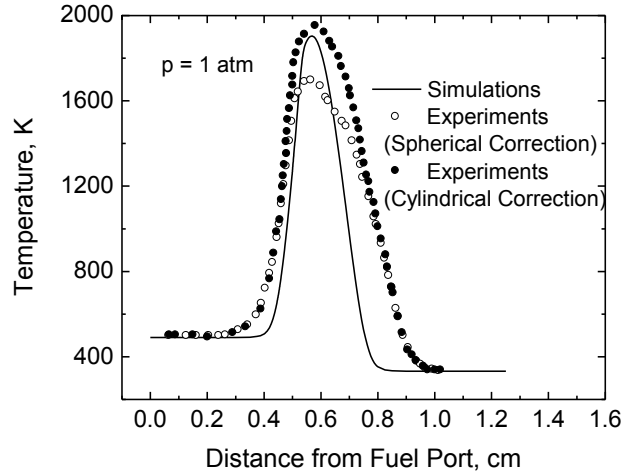


**Figure 5: Comparison of the predicted and measured [33] temperature profiles in a 1.52% n-dodecane/75% oxygen diffusion flame at a strain rate of  $105 \text{ s}^{-1}$ .**

### 3.2 3D Simulations at CI Engine Conditions

Further validation of the 103-species n-dodecane mechanism is performed in a 3D constant volume combustion chamber under CI engine conditions. Experimental data for comparison is obtained from Sandia National Laboratories [8,9] where a constant volume quiescent preburn-type combustion vessel was used to generate high-temperature and high-pressure gases. The conditions are noted in Table 1. A premixed combustible mixture was spark ignited; the combustion products cool over a long time. Once the desired pressure and temperature are reached, the diesel fuel injector was triggered and fuel injection occurs. Pickett et al. [8] investigated the influence of ambient temperature on ignition delay and flame LOL. This experimental dataset is used for extensive validation of the reduced n-dodecane mechanism as presented earlier. In addition, liquid length and vapor penetration data under non-reacting conditions is also provided. This data is used for benchmarking the non-reacting simulations to ensure that fuel-air distribution is accurately predicted by the spray models.

Parameter	Quantity
Fuel	n-dodecane
Nozzle outlet diameter	90 $\mu\text{m}$
Nozzle K-factor	1.5
Nozzle shaping	Hydro-eroded
Discharge coefficient	0.86
Fuel injection pressure	150 MPa
Fuel injection temperature	363 K
Injection duration	1.5 ms
Injected fuel mass	3.5 mg
Injection rate shape	Square
Ambient gas temperature	800 - 1200 K
Ambient gas density	22.8 $\text{Kg/m}^3$
Ambient Oxygen Concentration	15 %

**Table 1: n-dodecane operating conditions at Sandia National Laboratories [7,8,9].**

Validations under non-reacting conditions are first presented followed by those under reacting conditions. This is motivated by the fact that the fuel distribution (equivalence ratio) needs to be accurately predicted prior to further validation of reaction mechanism. Since liquid penetration, vapor penetration, LOL, and ignition delay data will be used for validation of the mechanism, these parameters will be first defined here. In simulations, liquid penetration is defined as the axial location encompassing 97% of the injected mass at that instant of time. Vapor penetration at any time is determined from the farthest downstream location of 0.05% fuel mass-fraction contour. Flame LOL is determined by the nearest upstream location of temperature

$\geq 2200$  K contour. Ignition delay is defined as the time from start of injection to the time when temperatures above 2000K are first observed in any computational cell.

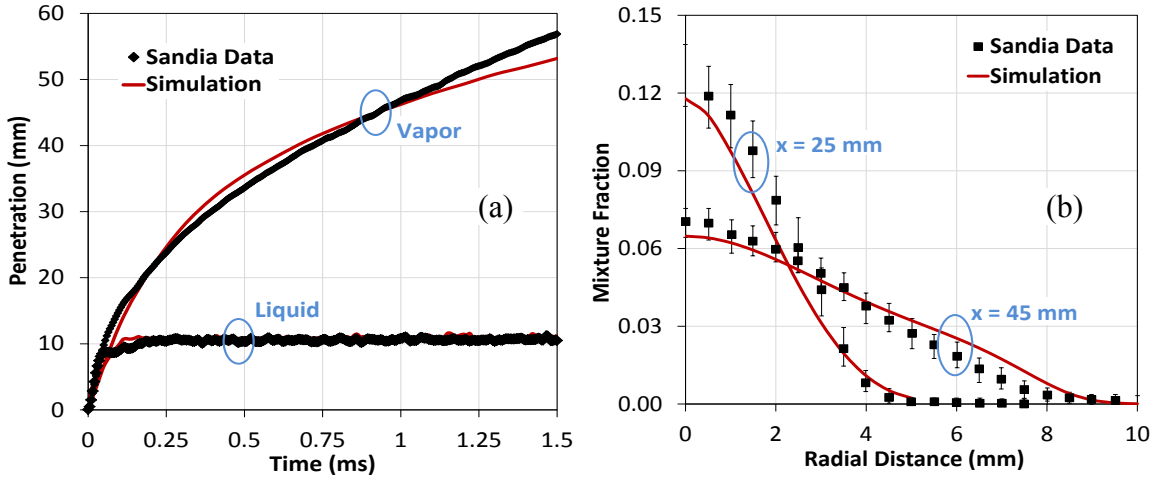


**Figure 6: Measured [7] and predicted (a) liquid spray penetration and vapor penetration vs. time, (b) mixture fraction distribution vs. radial distance at two different axial positions, for conditions depicted in Table 1 at an ambient temperature of 900K.**

Figure 6a presents predicted and measured liquid spray and fuel vapor penetration at different times after the start of injection (ASI) at an ambient temperature of 900K. Spray penetration initially increases with time and then stabilizes at a quasi-steady value, which is called the liquid length. Hence, beyond this axial distance, liquid fuel is absent. The fuel vapor penetration though increases with time and is instrumental in fuel-ambient air mixing. It is seen that the simulations are able to capture the liquid spray and vapor penetration characteristics very well. Figure 6b presents the mixture fraction distribution vs. radial position at two different axial positions of 25 mm and 45 mm from the injector nozzle at 1.0 ms ASI. In experiments the mixture fraction is calculated using Rayleigh scattering and the uncertainties in measurements are also noted. The fuel mass fraction was plotted for simulations since under non-reacting conditions the mixture fraction is equivalent to the fuel mass fraction. It is observed in Fig. 6b that the simulations are able to qualitatively capture the Gaussian nature of the mixture fraction distribution. In addition, the quantitative match is also excellent since the simulation results in general lie within the experimental uncertainties.

Figure 7a presents images of liquid fuel injected at different times ASI using Mie-scattering technique [7,8] and simulations corresponding to conditions depicted in Fig. 6a. The injected fuel droplets are plotted and the dashed line captures the liquid penetration at the noted time. The field of view is 20 mm x 8 mm in the axial and radial directions respectively. Distance from the injector is shown at the bottom. In general, the simulations are able to capture the experimentally observed fuel distribution contours fairly well and the experimentally observed value for liquid length of 10.6 mm (cf. Fig. 6a) is also predicted very well. Figure 7b plots the vapor contours at three different times ASI using Schlieren imaging [7,8] and simulations corresponding to conditions depicted in Fig. 6a. While Fig. 6a only captures the peak vapor penetration at different times ASI, Fig. 7b captures the contours of the vapor distribution. The field of view is 60 mm x 20 mm in the axial and radial directions respectively. At 0.5ms ASI, vapor penetration is over-predicted by the simulation, which is consistent with Fig. 6a. At 1.5ms ASI, vapor penetration is

under-predicted by the simulation and consequently dispersion is marginally over-predicted. Overall, simulations are able to capture the spray reacting conditions.

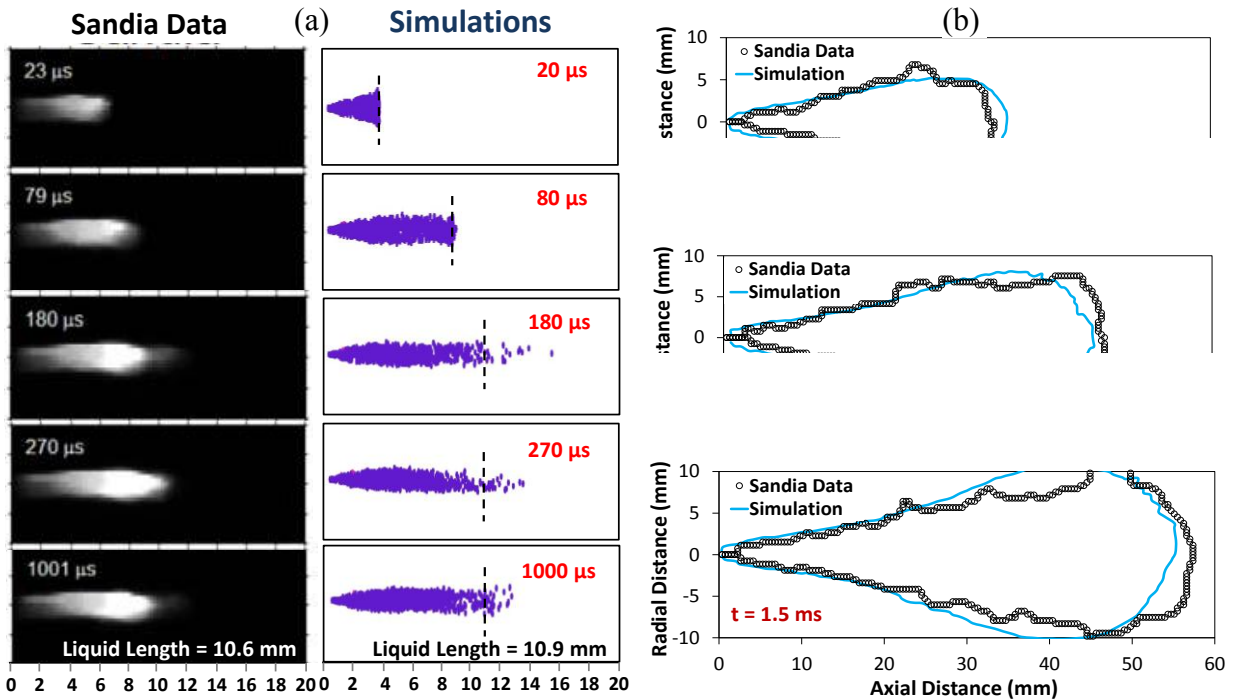


Figure 7: Measured [7] and predicted (a) liquid fuel spray distribution (b) vapor distribution, at different times ASI, for conditions depicted in Table 1 at an ambient temperature of 900K.

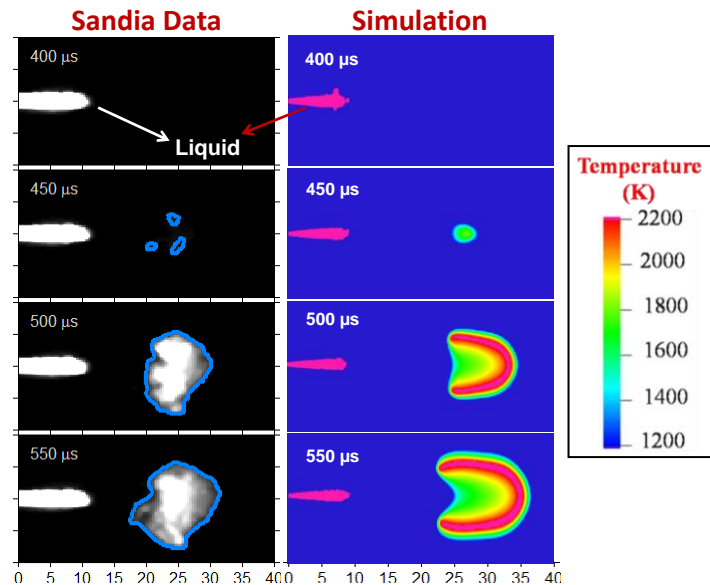
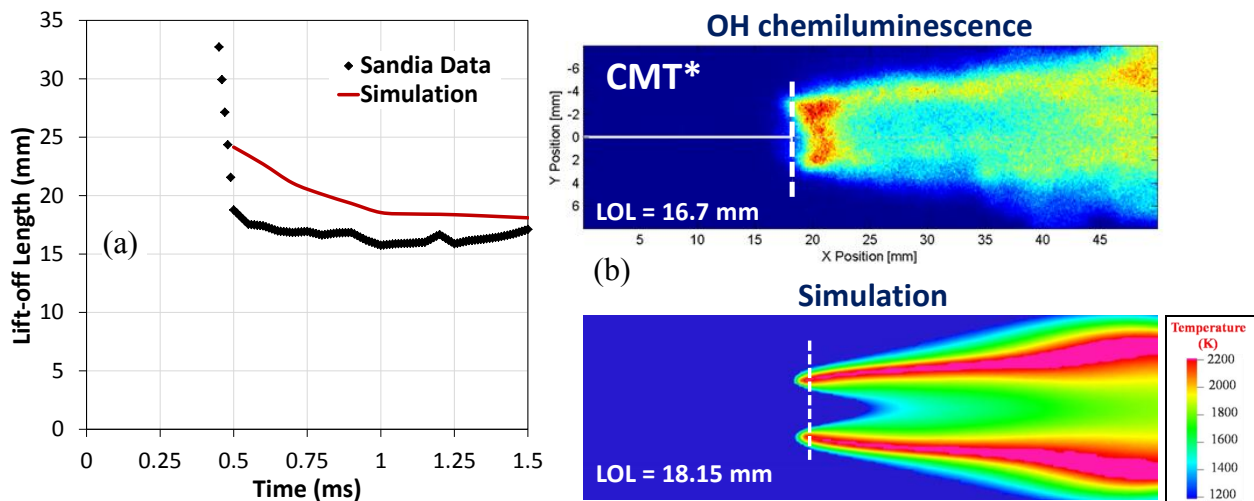


Figure 8: Measured [7,8] and predicted results on fuel spray distribution and ignition location and time, for conditions depicted in Table 1 at an ambient temperature of 900K.

Following the validations under non-reacting conditions, Figs. 8-11 show the validations under reacting conditions. Figure 8 compares liquid penetration and contour, ignition location

and time between experimental data [7,8] and simulations at conditions depicted in Table 1 at an ambient temperature of 900K. Liquid fuel distribution is measured using Mie-scattering and ignition delay is detected using high-speed direct imaging of natural luminosity. For the simulations, injected fuel droplets are plotted at different times ASI along with the temperature contours for the detection of ignition. Due to the axisymmetric nature of the spray and combustion processes, images are presented on a cut-plane through the center of the fuel jet. The field of view is 40 mm x 20 mm in the axial and radial directions, respectively. Distance from the injector is shown on the bottom. The simulations are able to capture the liquid fuel distribution very well, which is consistent with results presented above for non-reacting conditions (cf. Figs. 6a and 7a). In addition, the location and time of ignition is well captured by the simulation. The width and length of the flame is also well captured by the simulation under the ambient temperature condition investigated. At 500  $\mu$ s and 550  $\mu$ s the simulation is able to capture the experimental trend, i.e., the base of the flame moving upstream while the flame front moves downstream. It should be noted here that multiple ignition sites are not observed with the simulation since the turbulence model used is based on Reynolds Averaged Navier Stokes (RANS). A turbulence model based on large eddy simulations (LES) [34] may predict multiple ignition locations. However, the LES models are computationally expensive and beyond the scope of present study.



**Figure 9: Measured [7,35] and predicted (a) flame lift-off length vs. time ASI, (b) contour plot showing flame lift-off length at 1 ms ASI, for conditions depicted in Table 1 at an ambient temperature of 900K.**

Figure 9a plots measured and predicted flame lift-off length vs. time ASI at an ambient temperature of 900K. The above experimental images (cf. Fig. 8) show that the flame stabilizes between 15-20 mm shortly after auto-ignition, and the lift-off length remains at this position during rest of the injection event. The quasi-steady value of lift-off length was noted as 16.5 mm at Sandia [8] and 16.7 at Centro de Motores Termicos (CMT) [35]. Simulations on the other hand, predict that the base of the flame moves upstream and consequently stabilizes at about 1ms ASI. Previous studies by our group have also shown this tendency of RANS simulations predicting upstream movement of lift-off location [34]. The use of LES turbulence model [34] tends to predict multiple ignition locations thus capturing the volumetric auto-ignition phenomenon more accurately, which results in decreased upstream movement of flame lift-off

location. However, as mentioned above, LES simulations are beyond the scope of current study. The quasi-steady flame lift-off length value from simulation is noted to be 18.15 mm which is marginally higher than the experimental value. Fig. 9b plots the OH chemiluminescence measurement at CMT [35] and corresponding temperature contours from simulations at 1 ms ASI. The lift-off location is shown by white dashed lines in both experiment and simulation. The field of view is 50 mm x 17 mm in the axial and radial directions respectively. As mentioned above, simulation tends to over-predict the flame lift-off location under the ambient temperature of 900K. In general, the shape of the flame is well captured by the simulation.

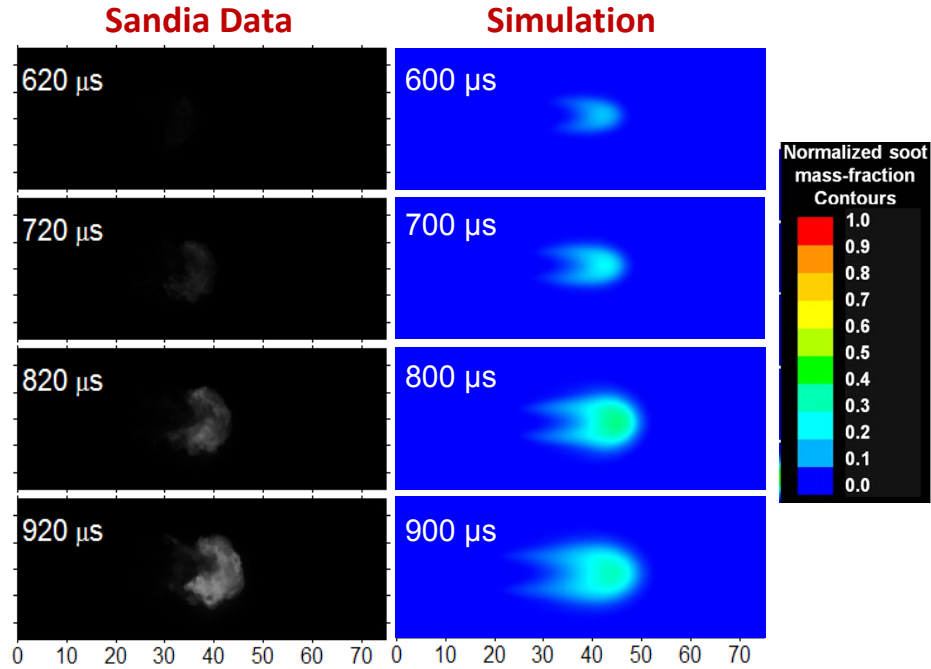


**Figure 10: Comparison of soot mole-fraction contours from simulations against the soot data using LII from Ref. [8] at different instances during the combustion process for conditions depicted in Table 1 at an ambient temperature of 900K.**

Planar laser-induced incandescence (PLII) images of soot [8] along a thin plane of the fuel jet were compared with the simulations in Fig. 10. Time ASI for each image is shown on the left thus the temporal evolution of a typical combustion event is seen. Distance from the injector is shown at the bottom. The field of view is 75 mm x 25 mm in the axial and radial directions respectively. The soot mass production within a computation cell is determined from a single-step competition between formation and oxidation rates of  $C_2H_2$  species, based on the Hiroyasu model [29]. This soot model has been extensively used in the literature. It can be seen that the predicted soot distributions agree well with the experimental results. The experimentally observed trend that soot generation occurs beyond the lift-off length location is also well captured by the simulation.

Figure 11 presents a comparison of the measured [7,35] and predicted flame LOL and ignition delays as a function of ambient temperature, calculated using the 103-species dodecane mechanism under conditions depicted in Table 1. Increased ambient temperatures results in decreased ignition delays as expected. Ignition delay is observed to be marginally over-predicted by the simulations at an ambient temperature of 1200 K. Ignition delay in a two-phase flow

consists of physical and chemical delays. Since the spray data, i.e., Sauter mean diameter (SMD), spray penetration etc., is not available at 1200 K, it is difficult to attribute the differences in the predicted ignition delay on the spray models or the n-dodecane reduced mechanism. An increase in ambient temperature (keeping ambient density constant) results in lowered flame LOL due to the increased chemical reactivity, which moves the ignition and flame stabilization locations upstream. It should be noted that in simulations for each ambient temperature case, LOL is noted at 1.0 ms ASI. In general, the reduced mechanism predicts the overall trends of LOLs very well.

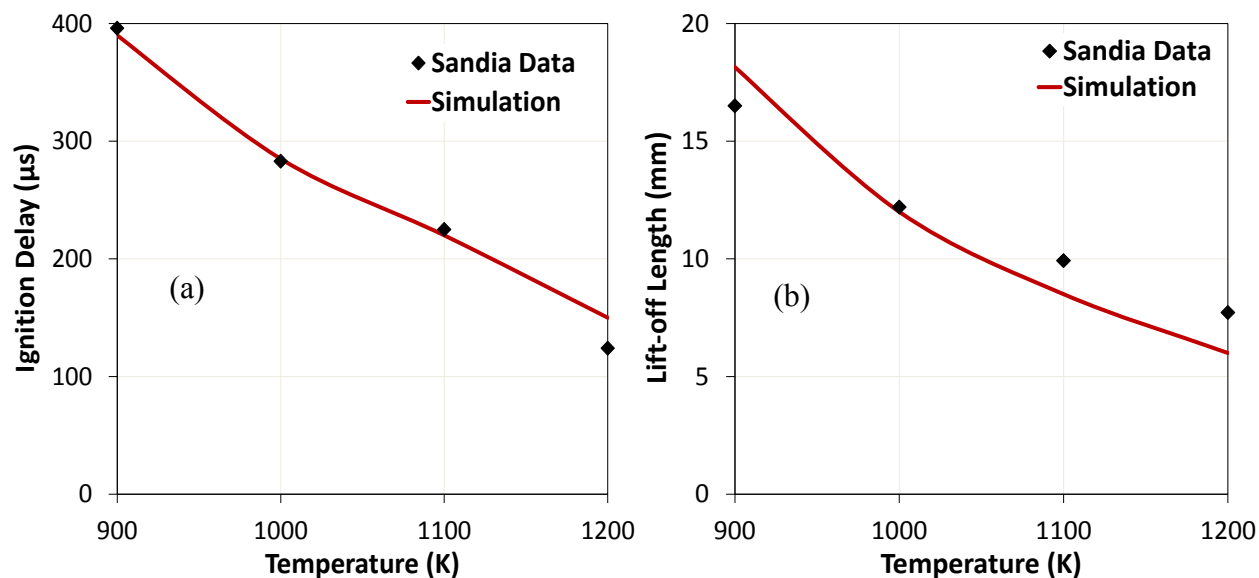


**Figure 11: Measured and predicted (a) ignition delay (b) flame lift-off length, vs. ambient temperature, for conditions depicted in Table 1.**

#### 4. Concluding Remarks

A 103-species skeletal mechanism for n-dodecane including low-temperature chemistry was derived from the detailed mechanism developed by the Lawrence Livermore National Laboratory. The mechanism reduction was performed using DRG-X and DRGASA techniques under CI engine relevant conditions. The skeletal mechanism was comprehensively validated against the detailed mechanism. It was shown that the small skeletal mechanism performs well over a wide range of parameters for both ignition and extinction applications. The reduced mechanism was further validated against experimental data for the shock-tube ignition delay, jet stirred reactors, and opposed flow flames. Extended validation was performed against 3-D turbulent spray combustion data at CI engine conditions obtained from ECN. First, spray validations were performed for predicting the fuel distribution in the combustion chamber against liquid penetration, vapor penetration, liquid length, and liquid and vapor contour data. Spray combustion simulation results show that the mechanism is versatile and robust since it performed satisfactorily in predicting the ignition delay and flame lift-off length, as well as the OH and soot concentration profiles under different ambient temperatures. As such the 103-species n-dodecane skeletal mechanism is suitable for multi-dimensional engine combustion simulations with diesel fuel.

## Acknowledgments

The work at University of Connecticut was supported by the National Science Foundation under Grant 0904771. Any opinions, findings, and conclusions or recommendations expressed in this material are those of the authors and do not necessarily reflect the views of the National Science Foundation.

The submitted manuscript has been created by UChicago Argonne, LLC, operator of Argonne National Laboratory (Argonne). Argonne, a U.S. Department of Energy Office of Science laboratory, is operated under Contract No. DE-AC02-06CH11357. The U.S. Government retains for itself, and others acting on its behalf, a paid-up, nonexclusive, irrevocable worldwide license in said article to reproduce, prepare derivative works, distribute copies to the public, and perform publicly and display publicly, by or on behalf of the Government.

## References

- [1] S.C. Kong, Y. Sun, R.D. Reitz, *Journal of Engineering for Gas Turbine and Power* 129 (2007) 245-251.
- [2] P.K. Senecal, K.J. Richards, E. Pomraning, T. Yang, M.Z. Dai, R.M. McDavid, M.A. Patterson, S. Hou, T. Shethaji, *SAE Paper* (2007) 2007-01-0159.
- [3] S. Som, S. "Development and Validation of Spray Models for Investigating Diesel Engine Combustion and Emissions;" PhD thesis, University of Illinois at Chicago; 2009.
- [4] X. You, F.N. Egolfopolous, H. Wang, *Proceedings of the Combustion Institute* 32 (2009) 403–410
- [5] C.K. Westbrook, W.J. Pitz, O. Herbinet, H.J. Curran, E.J. Silke, *Combustion and Flame* 156 (2009) 181–199.
- [6] S.S Vasu, D.F. Davidson, Z. Hong, V. Vasudevan, R.K. Hanson, *Proceedings of the Combustion Institute* 32 (2009) 173–180.
- [7] <http://www.sandia.gov/ecn/>
- [8] L.M. Pickett, C.L. Genzale, G. Bruneaux, L.M. Malbec, L. Hermant, C. Christiansen, J. Schramm, *SAE Paper* (2010) 2010-01-2106.
- [9] L.M. Pickett, J. Manin, C.L. Genzale, D.L. Sieber, M.P.B. Musculus, C.A. Idicheria, *SAE Paper* (2011) 2011-01-0686.
- [10] <http://www.sandia.gov/ecn/proceed/proceedECN1.php>
- [11] <http://www.sandia.gov/ecn/proceed/ECN1/SprayA.pdf>
- [12] <http://www.sandia.gov/ecn/proceed/ECN1/baselinen-heptane.pdf>
- [13] T.F. Lu, C.K. Law, *Proceedings of the Combustion Institute* 30 (2005) 1333-1341.
- [14] Z. Luo, T. Lu, M.J. Maciaszek, S. Som, and D.E. Longman, *Energy Fuel*, 24 (2010) 6283–6293.
- [15] T. Lu, M. Plomer, Z. Luo, S.M. Sarathy, W.J. Pitz, S. Som, D.E. Longman, *7<sup>th</sup> US National Combustion Meeting Atlanta, GA* (2011).
- [16] X.L. Zheng, T.F. Lu, C.K. Law, *Proceedings of the Combustion Institute* 31 (2007) 367-375.
- [17] R. Sankaran, E.R. Hawkes, J.H. Chen, T. Lu, C.K. Law, *Proceedings of the Combustion Institute* 31 (2007) 1291-1298.
- [18] Z. Luo, M. Plomer, T. Lu, S. Som, D.E. Longman, S.M. Sarathy, W.J. Pitz, *A reduced mechanism for biodiesel surrogates for compression ignition engine applications*, Submitted to *Fuel* 2011.
- [19] K.J. Richards, P.K. Senecal, E. Pomraning, *CONVERGE<sup>TM</sup> (Version 1.2) Manual* (2008), Convergent Science Inc., Middleton, WI.
- [20] S. Som, D.E. Longman, *Energy and Fuel* 25 (2011) 1373-1386.
- [21] S. Som, S.K. Aggarwal, *Combustion and Flame* 157 (2010) 1179-1193.
- [22] S. Som, D.E. Longman, A.I. Ramirez, S.K. Aggarwal, *Fuel* 89 (2010) 4014-4024.
- [23] S. Som, A.I. Ramirez, D.E. Longman, S.K. Aggarwal, *Fuel* 90 (2011) 1267-1276.
- [24] R.D. Reitz, *Atomization and Spray Technology* 3 (1987) 309-337.
- [25] M.A. Patterson, R.D. Reitz, *SAE Paper* (1998) 980131.
- [26] D.P. Schmidt, C.J. Rutland, *Journal of Computational Physics* 164 (2000) 62-80.
- [27] S.L. Post, J. Abraham, *International Journal of Multiphase Flow* 28 (2002) 997-1019.

- [28] P.K. Senecal, E. Pomraning, K.J. Richards, T.E. Briggs, C.Y. Choi, R.M. McDavid, M.A. Patterson, *SAE Paper* (2003) 2003-01-1043.
- [29] J.B. Heywood, *Internal Combustion Engine Fundamentals*, McGraw-Hill Inc., 1998.
- [30] D.F. Davidson, D.R. Haylett, R.K. Hanson, *Combustion and Flame* 155 (2008) 108-117.
- [31] H.S. Shen, J. Steinberg, J. Vanderover, M.A. Oehlschlaeger, *Energy Fuels* 23 (2009) 2482-2489.
- [32] O. Herbinet, P.M. Marquaire, F. Battin-Leclerc, R. Fourneta, *Journal of Analytical and Applied Pyrolysis* 78 (2007) 419-429.
- [33] J.A. Cooke, M. Bellucci, M.D. Smooke, A. Gomez, A. Violi, T. Faravelli, E. Ranzi, *Proceedings of the Combustion Institute* 30 (2005) 439-446.
- [34] S. Som, D.E. Longman, Z. Luo, M. Plomer, T. Lu, P.K. Senecal, E. Pomraning, *Proceedings of the ASME 2011 Internal Combustion Engine Division Fall Technical Conference* (2011) ICEF2011-60051.
- [35] <http://www.cmt.upv.es/ECN07.aspx>